Research Article | Vol. 26, No. 5 | 5 Mar 2018 | OPTICS EXPRESS 6114

Optics EXPRESS

Optical performance of large-area crystalline coatings

MANUEL MARCHIÒ,[1,2,*] RAFFAELE FLAMINIO,[1,2,6] LAURENT PINARD,[3] DANIÉLE FOREST,[3] CHRISTOPH DEUTSCH,[4] PAULA HEU,[5] DAVID FOLLMAN,[5] AND GARRETT D. COLE[4,5]

[1]*Department of Astronomy, The University of Tokyo, Tokyo 113-8654, Japan*
[2]*National Astronomical Observatory of Japan, Tokyo 181-8588, Japan*
[3]*Laboratoire des Matériaux Avancés—CNRS/IN2P3, F-69622 Villeurbanne, France*
[4]*Crystalline Mirror Solutions GmbH, 1010 Vienna, Austria*
[5]*Crystalline Mirror Solutions LLC, Santa Barbara, CA 93101, USA*
[6]*now at: Laboratoire d'Annecy de Physique des Particules, 74940 Annecy-le-Vieux, France*
[*]*manuel.marchio@nao.ac.jp*

Abstract: Given their excellent optical and mechanical properties, substrate-transferred crystalline coatings are an exciting alternative to amorphous multilayers for applications in precision interferometry. The high mechanical quality factor of these single-crystal interference coatings reduces the limiting thermal noise in precision optical instruments such as reference cavities for narrow-linewidth laser systems and interferometric gravitational wave detectors. In this manuscript, we explore the optical performance of GaAs/AlGaAs crystalline coatings transferred to 50.8-mm (2-inch) diameter fused silica and sapphire substrates. We present results for the transmission, scattering, absorption, and surface quality of these prototype samples including the defect density and micro-roughness. These novel coatings exhibit optical performance on par with state-of-the-art dielectric structures, encouraging further work focused on the fabrication of larger optics using this technique.

OCIS codes: (300.1030) Absorption; (260.1180) Crystal optics; (310.1620) Interference coatings; (160.4670) Optical materials; (290.5820) Scattering measurements; (160.6000) Semiconductor materials.

References and links

1. The LIGO Scientific Collaboration, "Advanced LIGO," Class. Quantum Grav., **32**, 74001–74041 (2015).
2. F. Acernese, M. Agathos, K. Agatsuma, D. Aisa, N. Allemandou, A. Allocca, J. Amarni, P. Astone, G. Balestri, G. Ballardin, F. Barone, J-P. Baronick, M. Barsuglia, A. Basti, F. Basti, Th S. Bauer, V. Bavigadda, M. Bejger, M G. Beker, C. Belczynski, D. Bersanetti, A. Bertolini, M. Bitossi, M A. Bizouard, S. Bloemen, M. Blom, M. Boer, G. Bogaert, D. Bondi, F. Bondu, L. Bonelli, R. Bonnand, V. Boschi, L. Bosi, T. Bouedo, C. Bradaschia, M. Branchesi, T. Briant, A. Brillet, V. Brisson, T. Bulik, H J. Bulten, D. Buskulic, C. Buy, G. Cagnoli, E. Calloni, C. Campeggi, B. Canuel, F. Carbognani, F. Cavalier, R. Cavalieri, G. Cella, E. Cesarini, E Chassande-Mottin, A. Chincarini, A. Chiummo, S. Chua, F. Cleva, E. Coccia, P-F. Cohadon, A. Colla, M. Colombini, A. Conte, J-P. Coulon, E. Cuoco, A. Dalmaz, S. D'Antonio, V. Dattilo, M. Davier, R. Day, G. Debreczeni, J. Degallaix, S. Deléglise, W Del Pozzo, H. Dereli, R De. Rosa, L Di Fiore, A. Di Lieto, A. Di Virgilio, M. Doets, V. Dolique, M. Drago, M. Ducrot, G. Endröczi, V. Fafone, S. Farinon, I. Ferrante, F. Ferrini, F. Fidecaro, I. Fiori, R. Flaminio, J-D. Fournier, S. Franco, S. Frasca, F. Frasconi, L. Gammaitoni, F. Garufi, M. Gaspard, A. Gatto, G. Gemme, B. Gendre, E. Genin, A. Gennai, S. Ghosh, L. Giacobone, A. Giazotto, R. Gouaty, M. Granata, G. Greco, P. Groot, G M. Guidi, J. Harms, A. Heidmann, H. Heitmann, P. Hello, G. Hemming, E. Hennes, D. Hofman, P. Jaranowski, R J G. Jonker, M. Kasprzack, F. Kéfélian, I. Kowalska, M. Kraan, A. Królak, A. Kutynia, C. Lazzaro, M. Leonardi, N. Leroy, N. Letendre, T G F. Li, B. Lieunard, M. Lorenzini, V. Loriette, G. Losurdo, C. Magazzú, E. Majorana, I. Maksimovic, V. Malvezzi, N. Man, V. Mangano, M. Mantovani, F. Marchesoni, F. Marion, J. Marque, F. Martelli, L. Martellini, A. Masserot, D. Meacher, J. Meidam, F. Mezzani, C. Michel, L. Milano, Y. Minenkov, A. Moggi, M. Mohan, M. Montani, N. Morgado, B. Mours, F. Mul, M F. Nagy, I. Nardecchia, L. Naticchioni, G. Nelemans, I. Neri, M. Neri, F. Nocera, E. Pacaud, C. Palomba, F. Paoletti, A. Paoli, A. Pasqualetti, R. Passaquieti, D. Passuello, M. Perciballi, S. Petit, M. Pichot, F. Piergiovanni, G. Pillant, A. Piluso, L. Pinard, R. Poggiani, M. Prijatelj, G A. Prodi, M. Punturo, P. Puppo, D S. Rabeling, I. Rácz, P. Rapagnani, M. Razzano, V. Re, T. Regimbau, F. Ricci, F. Robinet, A. Rocchi, L. Rolland, R. Romano, D. Rosińska, P. Ruggi, E. Saracco, B. Sassolas, F. Schimmel, D. Sentenac, V. Sequino, S. Shah, K. Siellez, N. Straniero, B. Swinkels, M. Tacca, M. Tonelli, F. Travasso, M. Turconi, G. Vajente, N. van Bakel, M. van Beuzekom, J F J. van den Brand, C Van Den.

#315287 https://doi.org/10.1364/OE.26.006114
Journal © 2018 Received 11 Dec 2017; revised 21 Jan 2018; accepted 23 Jan 2018; published 28 Feb 2018

Optics EXPRESS

Broeck, M V. van der Sluys, J. van Heijningen, M. Vasúth, G. Vedovato, J. Veitch, D. Verkindt, F. Vetrano, A. Viceré, J-Y. Vinet, G. Visser, H. Vocca, R. Ward, M. Was, L-W. Wei, M. Yvert, A. Zadrozny, and J-P. Zendri, "Advanced Virgo: a second-generation interferometric gravitational wave detector," Class. Quantum Grav. **32**(2), 1 (2015).
3. K. Somiya, "Detector configuration of KAGRA–the Japanese cryogenic gravitational-wave detector," Class. Quantum Grav. **29**, 124007 (2012).
4. G. M. Harry, A. M. Gretarsson, P. R. Saulson, S. E. Kittelberger, S. D. Penn, W. J. Startin, S. Rowan, M. M. Fejer, D. R. M. Crooks, G. Cagnoli, J. Hough, and N. Nakagawa, "Thermal noise in interferometric gravitational wave detectors due to dielectric optical coatings," Class. Quantum Grav. **19**(5), 897 (2002).
5. L. Pinard, C. Michel, B. Sassolas, L. Balzarini, J. Degallaix, V. Dolique, R. Flaminio, D. Forest, M. Granata, B. Lagrange, N. Straniero, J. Teillon, and G. Cagnoli, "Mirrors used in the LIGO interferometers for first detection of gravitational waves," Appl. Opt. **56**(4), C11–C15 (2017).
6. R. Flaminio, J. Franc, C. Michel, N. Morgado, L. Pinard, and B. Sassolas, "A study of coating mechanical and optical losses in view of reducing mirror thermal noise in gravitational wave detectors," Class. Quantum Grav. **27**(8), 84030 (2010).
7. P. R. Saulson, "Thermal noise in mechanical experiments," Phys. Rev. D **42**(8), 2437 (1990).
8. M. Granata, E. Saracco, N. Morgado, A. Cajgfinger, G. Cagnoli, J. Degallaix, V. Dolique, D. Forest, J. Franc, C. Michel, L. Pinard, and R. Flaminio, "Mechanical loss in state-of-the-art amorphous optical coatings," Phys. Rev. D **93**, 012007 (2016).
9. G. D. Cole, W. Zhang, M. Martin, J. Ye, and M. Aspelmeyer, "Tenfold reduction of Brownian noise in high-reflectivity optical coatings," Nature Photonics **7**(8), 644-–650 (2013).
10. G. D. Cole, "Cavity optomechanics with low-noise crystalline mirrors," SPIE Optics & Photonics, Optical Trapping and Optical Micromanipulation IX, San Diego, CA, USA, 12–16 August 2012 [8458-07].
11. G. D. Cole, P. Heu, D. Follman (CMS LLC); C. Deutsch, T. Zederbauer, and C. Pawlu (CMS GmbH), "CMS Inspection report, Crystalline coatings on Suprasil fused silica," (personal communication, 2016).
12. G. D. Cole, P. Heu, D. Follman (CMS LLC); C. Deutsch, T. Zederbauer, and C. Pawlu (CMS GmbH), "CMS Inspection report, Crystalline coatings on sapphire," (personal communication, 2016).
13. SHIMADZU UV-VIS-NIR Spectrophotometer Solidspec-3700 datasheet, https://www.ssi.shimadzu.com/products/literature/Spectroscopy/C101-E101D.pdf
14. B. Cimma, D. Forest, P. Ganau, B. Lagrange, J-M. Mackowski, C. Michel, J-L. Montorio, N. Morgado, R. Pignard, L. Pinard, and A. Remillieux, "Original optical metrologies of large components," Proc. SPIE **5252**, Optical Fabrication, Testing, and Metrology, 322 (2004).
15. E. Welsch and D. Ristau, "Photothermal measurements on optical thin films," Appl. Opt. **34**(31), 7239–7253 (1995);
16. W. B. Jackson, N. M. Amer, A. C. Boccara, and D. Fournier, "Photothermal deflection spectroscopy and detection," Appl. Opt. **20**(8), 1333–1344 (1981);
17. V. Loriette and C. Boccara, "Absorption of low-loss optical materials measured at 1064 nm by a position-modulated collinear photothermal detection technique," Appl. Opt. **42**(4), 649–656 (2003)
18. G. D. Cole, W. Zhang, B. J. Bjork, D. Follman, P. Heu, C. Deutsch, L. Sonderhouse, J. Robinson, C. Franz, A. Alexandrovski, M. Notcutt, O. H. Heckl, J. Ye, and M. Aspelmeyer, "High-performance near- and mid-infrared crystalline coatings," Optica, **3**(6) 647–656 (2016).
19. The VIRGO Collaboration, "The VIRGO large mirrors: a challenge for low loss coatings," Class. Quantum Grav. **21** S935-–S945 (2004).
20. T. D. B. Jacobs, T. Junge, and L. Pastewka, "Quantitative characterization of surface topography using spectral analysis," Surface Topography: Metrology and Properties, **5**(1), 013001 (2017).
21. C. Deumié, R. Richier, P. Dumas, and Claude Amra, "Multiscale roughness in optical multilayers: atomic force microscopy and light scattering," Appl. Opt. **35**(28), 5583–5594 (1996)

1. Introduction

Interferometric gravitational wave detectors such as Advanced LIGO [1], Advanced Virgo [2], and KAGRA [3] are among the most precise optical instruments ever constructed. Operating with record levels of displacement sensitivity, these systems are affected by many noise sources, such as seismic, thermal, and quantum noise. In the region of highest sensitivity, the current performance limitation is thermal noise, driven primarily by the mechanical loss of the high-reflectivity interference coatings and thus mirror Brownian noise [4]. Current detectors employ amorphous multilayer optical coatings, specifically metal oxides such as SiO_2 and TiO_2-alloyed Ta_2O_5, deposited by ion-beam sputtering [5, 6]. The excess noise in these systems can potentially be mitigated by the use of cryogenic cooling, though coating thermal noise will still remain as the limiting noise source. This is indeed the strategy of the Japanese detector KAGRA.

Brownian fluctuations are related to the coating mechanical dissipation. The thermal noise power spectral density is proportional to the Boltzmann constant k_B, the temperature T, the

Optics EXPRESS

mechanical loss angle ϕ, and the inverse of the frequency f, namely $G(f) \propto k_B T \cdot \phi \cdot 1/f$. The loss angle is the typical parameter that describes the coating mechanical quality in terms of its thermal noise and is defined as the imaginary part of the Young's modulus $E = E_0 [1 + i\phi]$ [7].

Current dielectric SiO_2/Ta_2O_5 multilayer high-reflectivity coatings deposited by ion beam sputtering (IBS) have loss angles of the order of 10^{-4} [8]. Pushing to lower loss angles will require the development of thin film materials with lower mechanical losses. Given the exceptionally high mechanical Qs found in bulk glasses (i.e. melt grown synthetic silica), through modifications to the deposition process, it may be possible to significantly reduce the mechanical dissipation in amorphous coatings. However, there is currently no clear route for achieving this yet, particularly in the case of the high index tantala layers. In contrast, high-reflectivity interference coatings based on substrate-transferred crystalline coatings have already demonstrated significant reductions in mechanical loss [9]. For this alternative solution, the challenge remains in scaling-up the manufacturing process. New optical materials for high-reflectivity coatings based on epitaxial or single-crystal materials are currently under investigation. Fabrication of such coatings is a technological challenge because optical applications such as atomic clocks and interferometric gravitational wave detectors require extremely high material purity, excellent surface quality, and, in the case of gravitational wave detectors, large coating diameters, typically at 20 cm and beyond. Substrate-transferred epitaxial multilayers based on single-crystal GaAs/AlGaAs heterostructures are promising candidates for alternative low-loss and high-reflectivity mirror coatings. Those coatings have been demonstrated to provide a tenfold reduction of Brownian noise, compared with amorphous coatings, with a reduction of the mechanical losses down to $\phi = 2.5 \times 10^{-5}$ at room temperature [9], and the potential for a loss angle below 5×10^{-6} at cryogenic temperatures [10].

In addition to low losses, high-precision laser interferometers require the mirrors to have very low total integrated scattering, below 10 ppm, to reduce stray-light phase noise. Since scattering is mainly caused by the surface roughness, the coating's micro-roughness must be very low. Moreover, absorption should be well below 1 ppm to minimize thermal lensing and to maintain a low base temperature in a cryogenic interferometer. Given the requirement of high-reflectivity, stringent thickness control is necessary to maintain the target transmission value. In this article we present the characterization of the optical performance of the first large-area (>1 cm diameter) crystalline coatings. This work was carried out to understand the current state of the technology and to provide motivation for further development activities. In Section 2 we describe the samples of this study in terms of fabrication technique, dimensions, thickness, and defects. In Section 3 we describe the measurement techniques and show the results.

2. Large-area crystalline coating

The samples measured for this study are high-reflectivity multilayer mirrors designed for a center wavelength of 1064 nm at room temperature. The interference coatings are based on a Bragg structure made of 35.5 doublets of epitaxial $GaAs/Al_{0.92}Ga_{0.08}As$ layers grown via molecular beam epitaxy (MBE). These layers are originally grown on a 15-cm diameter GaAs wafer with negligible lattice mismatch with the low-index $Al_{0.92}Ga_{0.08}As$ layer. The authors would like to stress that the maximum continuous diameter of the crystalline coating ultimately depends on the dimensions of the original GaAs growth wafer. Currently, 20-cm diameter GaAs wafers are commercially available and larger diameters up to 40 cm can be custom-grown. Following lithography and chemical etching processes, coating discs are defined and removed from the growth wafer. These disks are then directly bonded to the final optical substrate, in our case comprising planar fused silica and sapphire. Here, the substrates are 0.5-mm thick with a diameter of 50.8 mm (2 inches). The completed fused silica mirror is shown in Fig. 1.

Following the transfer process, the mirrors were inspected for bonding defects. Defect points larger than 100 µm are shown in Fig. 2 and Fig. 3. We also measured the number of defects using

Optics EXPRESS

a Micromap system (described in Section 3). Figure 4 shows the results of the defect mapping tests. The defect density is about 0.85 defects/mm^2, which is comparable with the coating of the End Test Masses of LIGO/Virgo whose defect density is about 0.7 defects/mm^2. However, we find that the total number of large defects (at the 100 µm or greater size scale) is higher than that of the test masses of Virgo. It is important to note that these samples were among the first crystalline coating prototypes manufactured at this size scale.

Note that the substrates employed for these tests, described in detail in Section 3, consisted of semiconductor-grade fused silica and c-axis oriented sapphire wafers. To the best of our knowledge, the surface quality of these samples was specified to guarantee excellent yield in bonding. However, in the course of our process development efforts, it became clear that the final substrates possessed properties that were not ideal for direct bonding. As a consequence of these non-ideal surface properties, coupled with a finite surface defect density of the epitaxial material, we were left with the aforementioned large defects at the bond interface. In terms of the limiting surface properties, the fused silica substrates exhibited larger than ideal micro-roughness, while the sapphire samples had an excessively poor surface figure (typically specified as bow/warp for these semiconductor-relevant substrates). The use of optimized epitaxial material with a lower surface defect density, in combination with high-quality "bulk" super-polished substrates would significantly reduce the defect density in such large-area optics employing crystalline coatings.

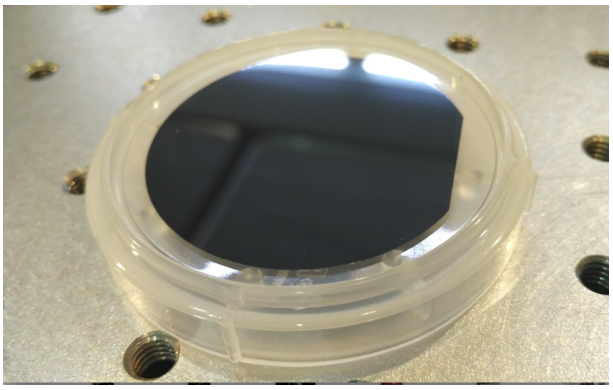

Fig. 1. Photograph of a substrate-transferred 35.5-period GaAs/ $Al_{0.92}Ga_{0.08}As$ multilayer on a 2-inch diameter × 0.5-mm thick fused silica substrate (lying on a plastic carrier).

Optics EXPRESS

Defect #	Size (μm)	Defect #	Size (μm)
1	200	10	63
2	85	11	55
3	62	12	121
4	186	13	185
5	65	14	98
6	60	15	117
7	75	16	76 &68
8	75	17	52
9	52	18	271
		19	51

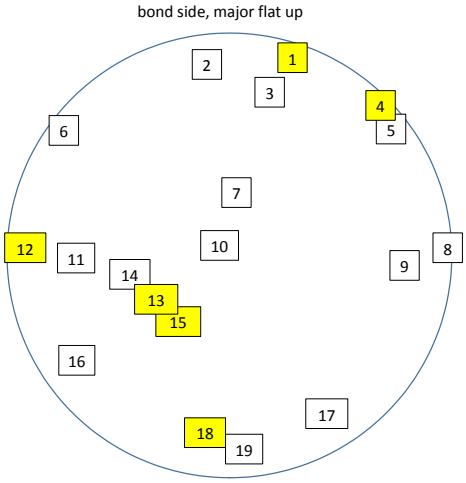

Fig. 2. Defects observed in the crystalline mirror coating transferred to fused silica [11]. Larger defects are highlighted in yellow. As described in the text, we identify a larger than desired count of visible defects. These defects are not intrinsic to the substrate-transfer coating process, but arise as a consequence of either macroscopic defects in the epitaxial films or, in this case, primarily from the poor surface quality (micro-roughness and figure) of the thin wafers and the resulting non-uniform propagation of the bond wave.

Defect	Size (μm)
A	216
B	690
C	1304
D	957
E	1462
F	941
G	171
H	875
I	250

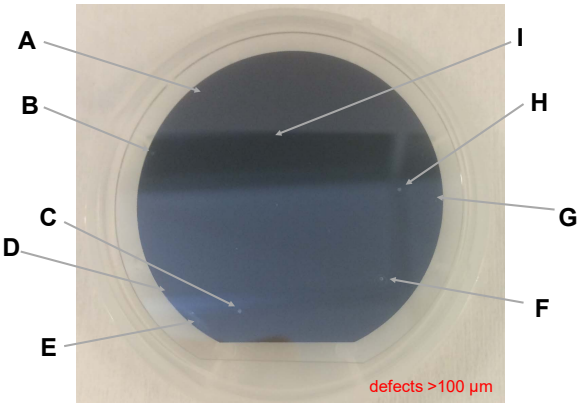

Fig. 3. Defects observed in the crystalline mirror coating transferred to sapphire. As with the sample transferred to the silica substrate, we identify visible defects as a consequence of non-ideal bonding conditions [12]. Defects larger than 100 μm are indexed with the letters A-I.

Optics EXPRESS

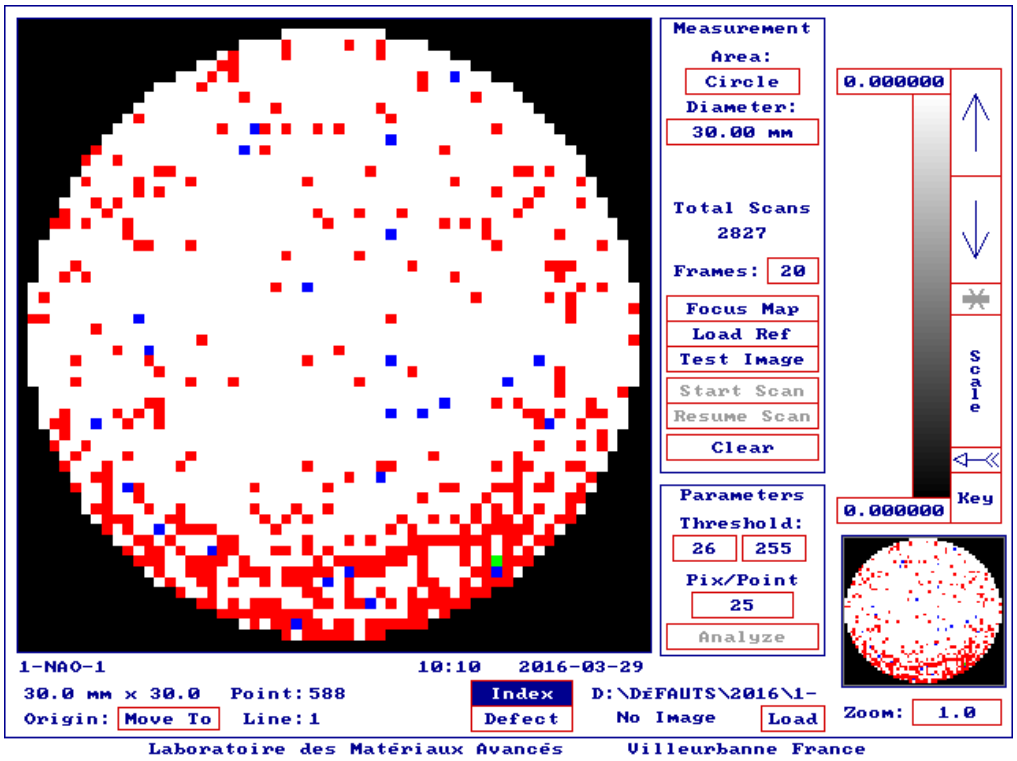

Fig. 4. Details of the defect count measured with the Micromap for the crystalline mirror coating transferred to sapphire. In this test we record 588 points, 1 line, and 21 regions covering the 2-inch diameter sample surface. The red dots correspond to small defects (< 5 µm) and blue dots to large defects (> 5 µm).

3. Measurements results

3.1. Transmission

The transmission spectra of the two crystalline mirror samples is measured with a commercial spectrophotometer, the SolidSpec-3700 [13]. The measured wavelength range spans from 890 to 1400 nm, with the resolution determined by the monochromator slit width. We chose 0.5 nm to have resolved spectrum peaks and a reasonable signal to noise ratio. We measure the transmission spectra, shown in Fig. 5, and compared it with calculated transmission curves based on a transmission matrix model. The amplitude of the oscillations is greater on the fused silica sample than the sapphire sample because of the larger difference in refractive index between the coating and the fused silica substrate. The transmission of the mirrors at 1064 nm was too low to be accurately measured by this spectrophotometer, so a 1064 nm laser and a detector were used to make this measurement. The transmission is 6 ppm for both substrates. This result is in very good agreement with the calculated transmission values. Note that the mirror stop bands of the two samples are slightly offset as each was produced in a separate growth run. As designed, these coatings have a nominal transmission of 9 ppm when transferred to a low-refractive-index substrate. Transmission matrix modeling shows that the lack of an AR coating on the backside of the silica and sapphire wafers yields the observed reduction in transmission to 7 ppm on fused silica and 6 ppm on sapphire due to the additional back-reflection from the substrate/air interface assuming constructive interference, yielding a reasonable match with the experimental values.

Optics EXPRESS

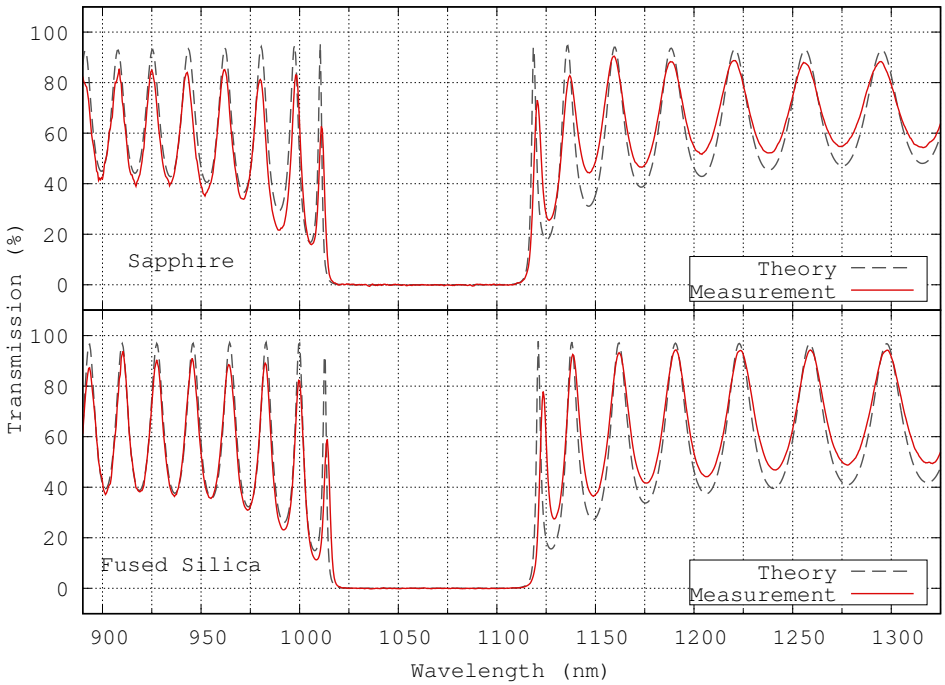

Fig. 5. Transmission spectra of the two crystalline mirror samples measured via spectrophotometry. The measured and theoretical transmission spectra are in very good agreement as shown in the plots. The slight offset in the mirror stopbands is a consequence of the use of material from two separate crystal growth runs for this experiment. Additionally, the satellite peaks show a variation in magnitude due to the different refractive indices of the substrates (fused silica n=1.449 and sapphire n=1.754 at 1064.0 nm).

3.2. *Absorption*

The absorption is measured with the photo-thermal deflection method. This technique has been used for many years and is well documented in the literature [14–17]. In this test, a 1 W pump laser at 1064 nm is modulated with an optical chopper, in order to periodically heat the sample. The temperature change is proportional to the laser power and to the absorption rate. Since the temperature gradient distribution induces a corresponding refractive index gradient, we use the resulting thermal-lens effect in order to sense the temperature change. A probe laser at 1310 nm (employed as GaAs is transparent at this wavelength) passes through the heated region which imposes a non-uniform wavefront phase shift that deflects the probe beam. Then, a position-sensitive detector measures the deflection, and this signal is demodulated by a lock-in amplifier to improve the signal to noise ratio. Since the demodulated signal is proportional to the temperature change, using the proper calibration, the absorption rate is measured. The calibration is done using a reference sample, a mirror on a silica substrate, with a known absorption rate of 8.1ppm. The signal is linear with the absorption, so the calibration procedure is a simple proportion. To get rid of long-time fluctuations of the experimental/environmental parameters, the calibration signal was measured on the same day of the measurement. The sensitivity is better than 1 ppm for fused silica samples. Sapphire has a higher thermal diffusivity, so the thermal lens effect is smaller and the sensitivity is worse. The absorption measurement is taken at a single point near the center of each sample.

The absorption is very low for both samples. In the case of the coating on the fused silica

Optics EXPRESS

substrate, the signal is ≤ 0.8 ppm which is comparable to the setup sensitivity. This result is similar to what is previously reported [18]. In the case of sapphire, the absorption signal is below the noise floor of the measurement. This is because of the above mentioned thermal diffusivity. As the two crystalline mirror coatings were grown separately, these absorption measurements also prove the excellent reproducibility of ultra-low absorption values for these coatings. The measurement of the absorption distribution over the entire sample surface was not done. This is scheduled for future measurements.

3.3. Scattering

To measure the scattering at 1064 nm, we use a complete angle scatter instrument named CASI [14]. In this setup, a 200 mW laser impinges on the mirror surface with an angle of 4°, then a photo-detector measures the scattering at 14° in the same plane of incidence . It is installed at 57 cm from the surface of the mirror, which means about 10 cm from the center of the reflected beam. This is the bidirectional reflectance distribution function (BRDF) value in sr^{-1} for those angles. A translation stage moves the sample in order to make a map of the scattering on the surface of the sample. The map resolution is 2 mm. In order to obtain the total integrated scattering (TIS) in ppm, the BRDF value should, in principle, be measured and integrated over all the scattering angles. Instead of doing this for each measurement, we employ a conversion curve. The conversion curve is generated by scanning the scattering intensity as a function of the scattering angle in the plane of incidence (for a given incidence angle). Then a rotational symmetry around the reflected beam (outside the plane of incidence) is assumed, so that the scattering can be easily integrated around the reflected beam. This assumption is true for low scattering optics. Figure 6 shows the map of the BRDF scattering of the fused silica sample on a 30 mm-diameter area and Fig. 7 shows the map of the BRDF scattering of the sapphire sample on a 35-mm diameter area.

The TIS averages on the maps are 9.5 ppm for the fused silica sample and 6 ppm for the sapphire sample. These values are comparable with currently used amorphous coatings and match the requirements for application in current gravitational wave interferometers [5].

3.4. Roughness

As scattering is mainly driven by surface roughness, we further investigated the surface quality of the samples. The roughness was measured with a commercial optical profilometer, Micromap 550. It measures the surface height by using a Fizeau interferometer [19]. The resolution of the map is 1.28 µm and the size is 300 µm × 300 µm. Raw 2D data are processed by removing the tilt and the curvature in order to get rid of most of the distortions that may come from the instrument optics. To realize such corrections, the map matrix is expanded on the Zernike polynomials space, then the first components are subtracted from the map: the Z_0^0 component for the offset, $Z_1^{+1,-1}$ components for the tilt, the Z_2^0 component for the radius of curvature, and the $Z_2^{+2,-2}$ components for the astigmatism. A Power Spectrum Density (PSD) of the surface height is used to quantify the properties of the surface. Although a 2D Fourier transform is calculated from the 2D data,

$$C^{2D}_{q_x,q_y} = \frac{1}{L_x L_y}\left|\frac{1}{L_x L_y}\sum_{x,y} h_{x,y} e^{-i(q_x x + q_y y)}\right|^2 \tag{1}$$

where $h_{x,y}$ is the surface height and L_x and L_y are the map dimensions, a 1D plot summarizes the main features of the surface. In particular, assuming that the roughness is isotropic, an easier-to-read 1D PSD is calculated from the 2D Fourier transform by averaging over all wavevectors where $|\vec{q}| = q$,

$$\mathrm{PSD}(q) = \frac{q}{2\pi^2}\int_0^{2\pi} C^{2D}(q\cos(\phi), q\sin(\phi))d\phi. \tag{2}$$

Optics EXPRESS

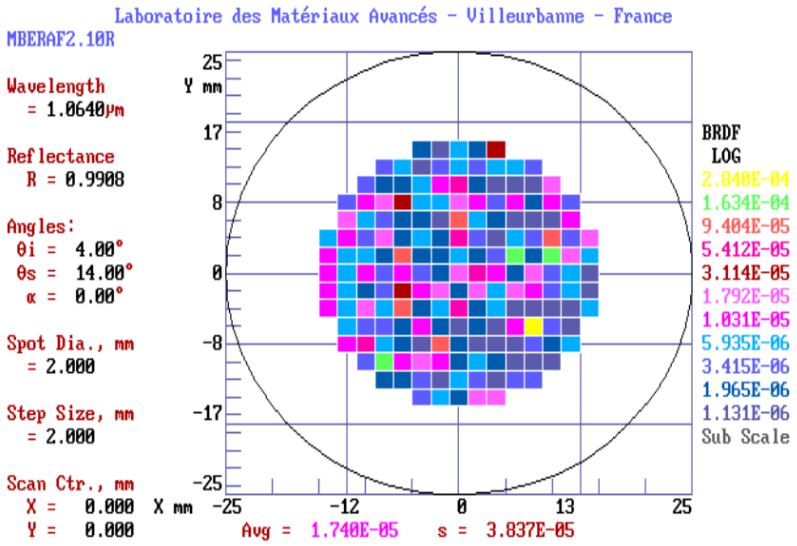

Fig. 6. BRDF map of the coating on fused silica substrate. The average corresponds to 9.5 ppm.

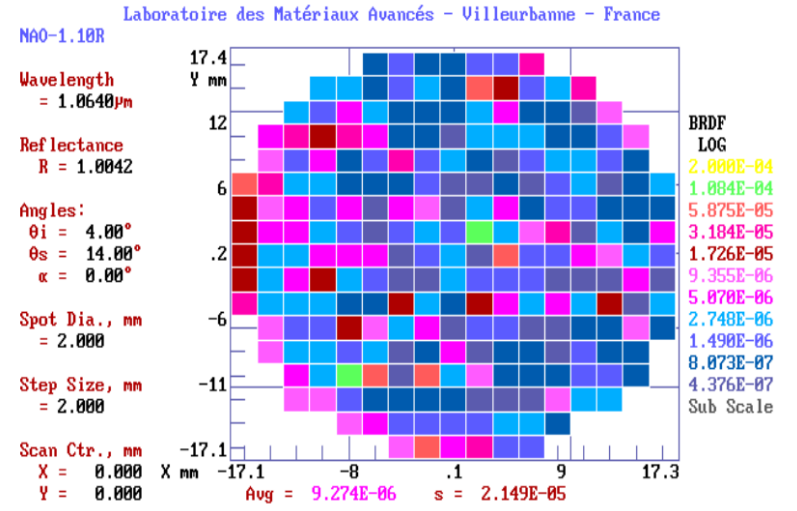

Fig. 7. BRDF map of the coating on sapphire substrate. The average corresponds to 6 ppm.

Optics EXPRESS

Finally the surface roughness is expressed as the root mean square (RMS) value, calculated as the standard deviation of the surface height or as the integral of the PSD [20, 21]. The roughness measurements are shown in Fig. 8 and the PSD is plotted in Fig. 9. The RMS roughness of the fused silica sample is 9.08 Å on substrate and 7.73 Å on coating, while for the sapphire sample it is 1.10 Å on the substrate and 1.08 Å on the coating. There is a difference of almost one order of magnitude between the coating roughness RMS of the fused silica sample and the sapphire sample. By looking at the PSD in Fig. 9, it can be seen that in general the roughness is limited by the substrate. Furthermore, we can notice that for the fused silica sample, at higher spatial frequencies, the coating roughness is lower than the one of the substrate. Also by looking at the maps in Fig. 8, it is clear that the coating on fused silica is smoother. A possible explanation of this is that in the case of fused silica, the coating does not perfectly follow the substrate surface roughness at short length-scales, so that the final mirror roughness is determined by the smoother surface of the coating.

It is important to note that the employed substrates, both the fused silica and sapphire wafers, are not optimized for bonding given their non-ideal surface quality, both in terms of excess micro-roughness (in the case of fused silica) and imperfect surface figure (typically quoted as bow and warp in semiconductor parlance). The relatively large bow/warp figures of >10 µm are caused by polishing and internal material stress, especially for the fused silica, of these thin wafers. Ultimately, the resulting non-ideal flatness drives many of the large defects in the samples due to non-uniform bond-wave propagation. Another driver for a subset of the defects is intrinsic/embedded defects in the epitaxial films themselves. Future tests would benefit from the use of high-quality bulk optical substrates with improved surface quality (micro-roughness and surface figure).

The optical performances of the two crystalline coating samples are summarized in Table 1.

Table 1. Tablecaption. Optical performances. Transmission, absorption and scattering measured at 1064 nm. The roughness is measured on a 300 µm length-scale.

Measurement	Coating on silica substrate	Coating on sapphire substrate
Transmission @1064 nm	6 ppm	6 ppm
Absorption @1064 nm	≤ 0.8 ppm	below the noise floor
Scattering @1064 nm	9.5 ppm	6 ppm
Coating Roughness	7.7 Å RMS	1.1 Å RMS
Substrate Roughness	9.1 Å RMS	1.1 Å RMS

4. Conclusion

These results, in particular the measured absorption of less than 1 ppm and the measured large-area scattering losses below 10 ppm, are remarkable. We find that substrate-transferred crystalline coatings are a promising alternative to ion-beam sputtering for applications in precision interferometry. Future efforts will focus on continued improvements in the manufacturing process for increasingly larger coating areas, with a major focus on reducing the density of large defects at the bond interface. In order to apply these coatings on gravitational wave detector test masses, the number of defects needs to be decreased, and, even more importantly, the size of the optics must be increased.

Our crystalline coating technology is admittedly new, but is maturing extremely rapidly, primarily driven by efforts relating to the development of ultrastable cavities for metrology (optical atomic clocks and inertial navigation being key drivers). For cm-scale coatings, the yield is now excellent [18]. Employing high quality epitaxial films together with super-polished

Optics EXPRESS

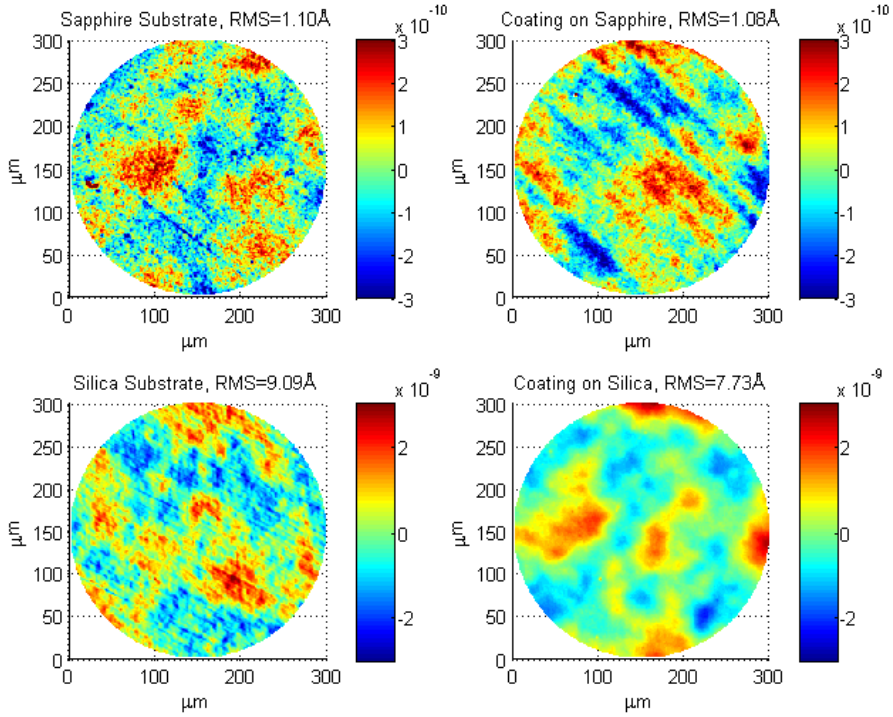

Fig. 8. Roughness of the substrate and coating for both of the sapphire and fused silica samples. The roughness of the sapphire sample remains effectively unchanged after the coating process. For fused silica though, a significant flattening effect is visible.

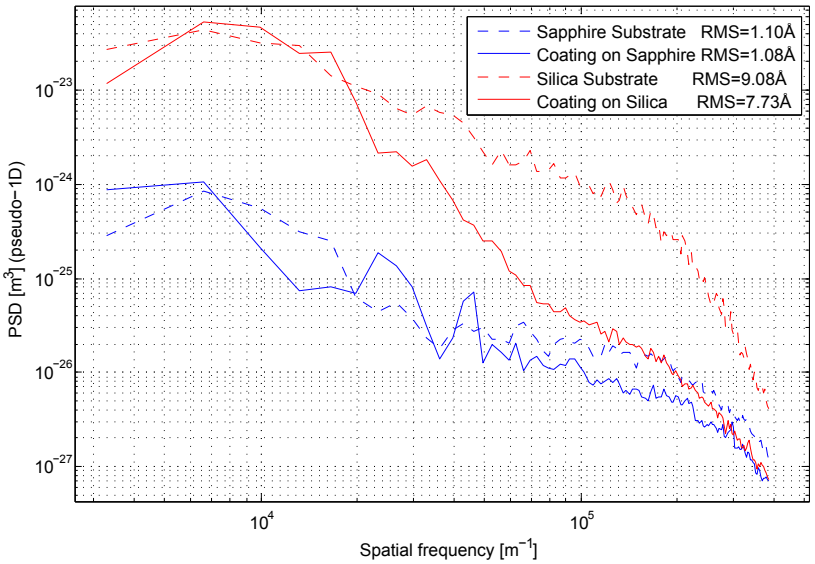

Fig. 9. Roughness PSD of uncoated (dashed lines) and coated (solid lines) sapphire (blue lines) and fused silica (red lines) samples. In the case of fused silica, the original substrate roughness is more than an order of magnitude larger for length scales around 10 µm.

Optics EXPRESS

substrates we can reach manufacturing yields of nearly 100% for defect-free bonded coatings. As the coating size increases, the process becomes challenging, but we are confident that similar yields can be achieved with dedicated tooling. Interestingly, upon initial contact, the coating is bonded by Van der Waals forces only and can be removed if the defect density doesn't meet the requirements. Only after a modest anneal (temperatures on the order of 100 °C) will the bond be permanently fused. Thus, critical substrates will not be destroyed by poor initial contact. At this time we are running aging studies on the long-term performance of our mirrors. This is driven by efforts related to space qualification of the optics as well as for some critical defense applications. We have ultrastable optical resonators deployed with coatings that are now a few years old with no reduction in finesse. GaAs is used extensively in micro- and optoelectronics (microwave transceivers and diode lasers based on GaAs represent multi-billion dollar per year commercial industries) and has proven to be a very robust material system. Thus, we anticipate no "show stoppers" in terms of degradation of our coatings. At this time we are not aware of any creep or crackle events in our bonded coatings, but dedicated long-term stability studies will have to be undertaken to confirm this.

These initial results on roughly 5-cm diameter coatings motivate us to continue developing this novel low-noise coating technology.

Funding

Japan Society for the Promotion of Science (26610073).

Acknowledgments

A portion of this work was performed in the UCSB Nanofabrication Facility.